Synthesis and Characterization of Divalent Manganese, Iron, and Cobalt Complexes in Tripodal Phenolate/N-Heterocyclic Carbene Ligand Environments

Martina Käß,[†] Johannes Hohenberger,[†] Mario Adelhardt,[†] Eva M. Zolnhofer,[†] Susanne Mossin,[‡] Frank W. Heinemann,[†] Jörg Sutter,[†] and Karsten Meyer*,[†]

[†]Department of Chemistry and Pharmacy, Inorganic Chemistry, Friedrich-Alexander-University Erlangen-Nuremberg, Egerlandstrasse 1, 91058 Erlangen, Germany

[‡]Department of Chemistry, Technical University of Denmark, Kemitorvet 207, 2800 Kgs. Lyngby, Denmark

Ⓢ *Supporting Information*

ABSTRACT: Two novel tripodal ligands, (BIMPN^{Mes,Ad,Me})$^-$ and (MIMPN^{Mes,Ad,Me})$^{2-}$, combining two types of donor atoms, namely, NHC and phenolate donors, were synthesized to complete the series of N-anchored ligands, ranging from chelating species with tris(carbene) to tris(phenolate) chelating arms. The complete ligand series offers a convenient way of tuning the electronic and steric environment around the metal center, thus, allowing for control of the complex's reactivity. This series of divalent complexes of Mn, Fe, and Co was synthesized and characterized by ^{1}H NMR, IR, and UV/vis spectroscopy as well as by single-crystal X-ray diffraction

studies. Variable-temperature SQUID magnetization measurements in the range from 2 to 300 K confirmed *high-spin* ground states for all divalent complexes and revealed a trend of increasing zero-field splitting |D| from Mn(II), to Fe(II), to Co(II) complexes. Zero-field ^{57}Fe Mössbauer spectroscopy of the Fe(II) complexes **3**, **4**, **8**, and **11** shows isomer shifts δ that increase gradually as carbenes are substituted for phenolates in the series of ligands. From the single-crystal structure determinations of the complexes, the different steric demand of the ligands is evident. Particularly, the molecular structure of **1**—in which a pyridine molecule is situated next to the Mn—Cl bond—and those of azide complexes **2**, **4**, and **6** demonstrate the flexibility of these mixed-ligand derivatives, which, in contrast to the corresponding symmetrical TIMEN^R ligands, allow for side access of, e.g., organic substrates, to the reactive metal center.
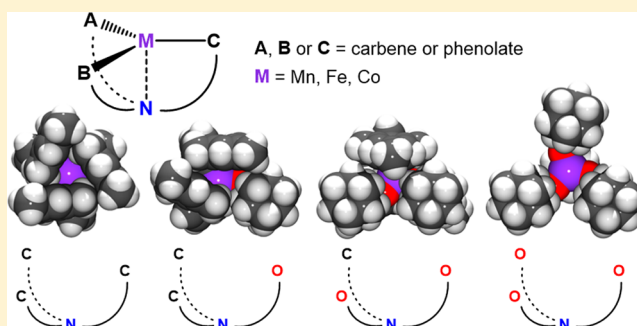
INTRODUCTION

Tripodal ligands provide a powerful platform for small molecule activation chemistry.[1−7] The ligand field splitting resulting from their trigonal coordination environment is suitable for the stabilization of highly unusual metal−ligand multiple bonds, even for relatively electron-rich mid to late transition metals.[7,8] This is most impressively exemplified by the synthesis of an Fe(II) imido complex,[9,10] the first terminal Co(III) imido,[11] and the first Fe(IV) nitrido species by Peters et al.[12]

Our laboratory routinely employs two different N-anchored tripodal ligand systems, the symmetrical tris(phenolate) ligand, ($^{R,R'}$ArO)$_3$N^{3-} (trianion of *tris*(3,5-R,R'-2-hydroxyphenyl)-methyl]amine, R, R' = alkyl)[13] and the tris(carbene) ligand TIMEN^R (*tris*[2-(3-R-imidazol-2-ylidene)ethyl]amine, R = alkyl, aryl).[14] A derivative of the tris(phenolate) ligand system with methyl substituents in the *ortho* and *para* positions of the phenol was first employed by Kleij and co-workers in the catalytic cycloaddition of CO$_2$ to epoxides and oxiranes with iron.[15] Uranium complexes of the tris(phenolate) ligand derivative (^{Ad,Me}ArO)$_3$N^{3-}, with adamantyl and methyl groups

in *ortho* and *para* positions, respectively, were employed to activate CO$_2$ and other heteroallene analogues.[16]

The ligand TIMEN^R (R = mesityl, 2,6-xylyl) enabled the stabilization and complete characterization of structurally characterized terminal Fe(IV) nitrido complexes.[17] A series of TIMEN^R (R = 2,6-xylyl) Mn nitrides in different oxidation states (III, IV, and V) have also recently been studied.[18] In all cases, the orientation of the imidazolydene substituents of the coordinated ligand is perpendicular to the metal−carbene plane, thus forming a narrow cavity that allows only axial access for small molecules to the reactive metal center. On the other hand, in the case of the cobalt peroxo complex of the xylyl ligand derivative,[19] two of the carbene arms are pushed apart, giving the complex an overall distorted octahedral symmetry that allows side access of organic substrates. Consequently, the complex was employed in O-atom transfer chemistry to organic substrates. In contrast, the 3-fold symmetrical iron nitrido and cobalt imido complexes of TIMEN^R (R = mesityl, 2,6-xylyl) did

not undergo any atom or group transfer chemistry. This could potentially be due to the inflexibility of the ligand. Instead, the RN^{2-} and N^{3-} ligands insert into the metal–carbene bond of the Co(III) imido and one-electron oxidized Fe(V) nitrido intermediates, forming bis(carbene) imine species (Scheme 1).[20,21]

Scheme 1. Insertion Reactions of the TIMEN^R (R = mesityl, 2,6-xylyl) Iron and Cobalt Imido[20] and Iron Nitrido Complexes[21]

R' = H, Me
a) M = Fe, Co,   R = Ar
b) M = Fe,

R' = H, Me
a) M = Fe, Co,   R = Ar
b) M = Fe,   R = H
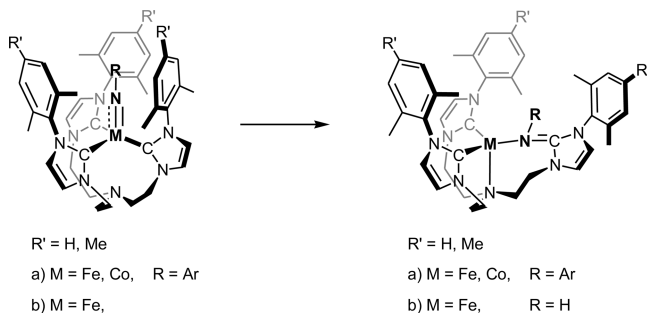
Consequently, we sought to reduce the steric bulk of the chelating ligand to enable side access of substrates to the functional entity. Our first strategy was to remove the *ortho*-CH_3 groups of the mesityl/xylyl substituents on the imidazolylidenes. However, the introduction of reactive hydrogens in these *ortho* positions leads to unexpected new reactivity, resulting in C–H activation and tris-metalation of the ligand.[22] Therefore, the design strategy was modified to exchange one or two carbene arms with phenolates. Introduction of phenolates still provides protection against bimolecular decomposition reactions. Nevertheless, the sterically encumbering *ortho*-adamantyl substituents on the phenolates are two atoms away from the coordinating O atom, whereas the NHC aryl substituents are attached to the N atom next to the carbene carbon atom; and hence, oriented perpendicularly to the Fe-tris(carbene) coordination plane. As a result, steric bulk of the *ortho* substituents on the phenolate is further away from the metal center and side access to the metal center ought to increase. These new ligands (BIMPN$^{R,R',R''}$)$^-$ (anion of *bis*[2-(3-R-<u>im</u>idazol-2-ylidene)ethyl-(3,5-R',R''-2-hydroxyphenyl)-methyl]am<u>in</u>e) and (MIMPN$^{R,R',R''}$)$^{2-}$ (dianion of *mono*[2-(3-R-<u>im</u>idazol-2-ylidene)ethyl-*bis*(3,5-R',R''-2-hydroxyphenyl)-methyl]am<u>in</u>e) (Chart 1) can be regarded as hybrid or crossover ligands of the N-anchored tris(carbene) and the tris(phenolate) ligand systems.

We herein report the synthesis and characterization of the novel, hybrid ligands (BIMPN$^{R,R',R''}$)$^-$ and (MIMPN$^{R,R',R''}$)$^{2-}$ and their coordination chemistry with divalent manganese, iron, and cobalt metal ions. While mixed NHC/phenolate ligands have been reported in the past,[23] most recently by Bercaw and co-workers,[24] (BIMPN$^{R,R',R''}$)$^-$ and (MIMPN$^{R,R',R''}$)$^{2-}$ are the first tripodal ligands that combine NHC and phenolate chelating arms. Together with the TIMEN^R and ($^{R',R''}$ArO)$_3$N^{3-} ligands, they provide a complete ligand series, ranging from N-anchored tris(carbene) to tris(phenolate) chelating arms.

■ **RESULTS AND DISCUSSION**

Ligand Synthesis. The tris(phenolate) ligand ((^{Ad,Me}ArO)$_3$N)$^{3-}$ was synthesized, according to the literature, in a *Mannich*-type procedure with 2-adamantyl-*p*-cresole[25] and hexamethylenetetramine with a catalytic amount of *p*-toluenesulfonic acid.[25] The tris(phenol) amine was deprotonated with NaOMe in toluene, from which the sodium salt precipitates as a colorless solid.
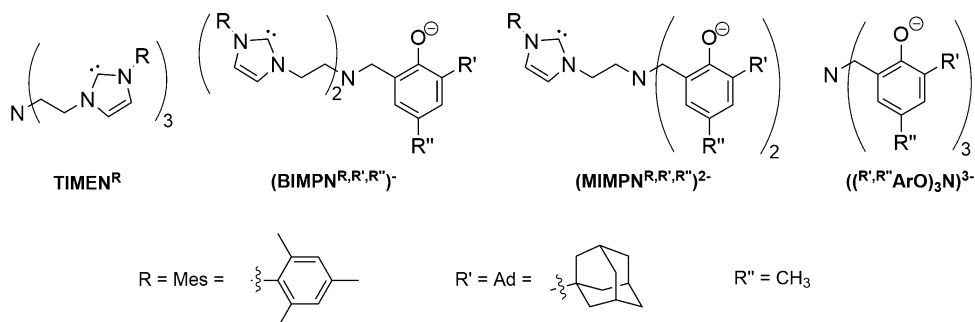
The syntheses of the two new hybrid ligand systems, namely, (BIMPN$^{R,R',R''}$)$^-$ and (MIMPN$^{R,R',R''}$)$^{2-}$, are summarized in Scheme 2. In the first step, the carbene units are attached to the nitrogen anchor in an S_N2 reaction of a halido-triethylamine with the substituted imidazole. The phenol is chloromethylated *via* a *Blanc* reaction, after which the amine nitrogen attacks the benzylic position to form the ligand precursors (H$_3$BIMPN$^{R,R',R''}$)$^{2+}$ and (H$_3$MIMPN$^{R,R',R''}$)$^+$, respectively. These ligand precursors are deprotonated with KOtBu in THF to yield the potassium salts of the free ligands in near quantitative yield.
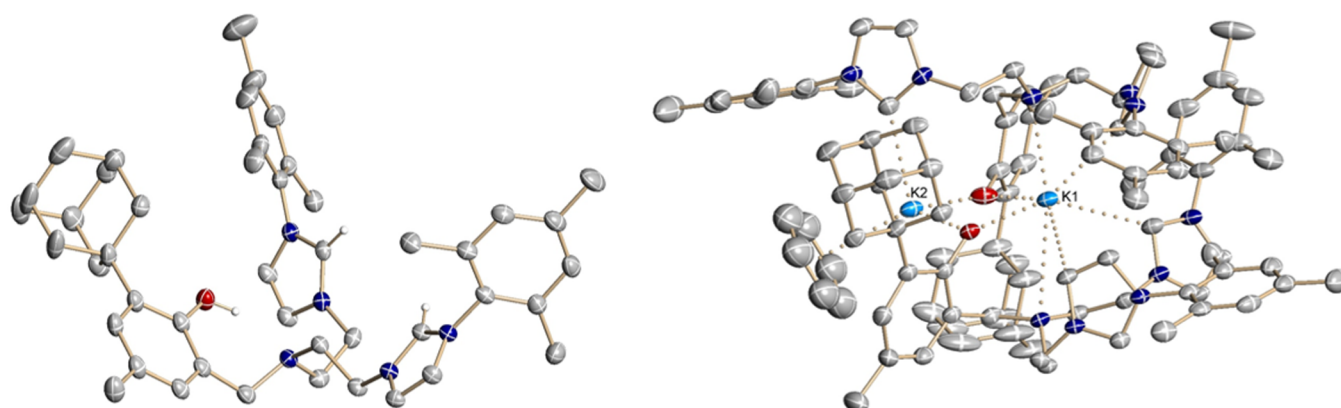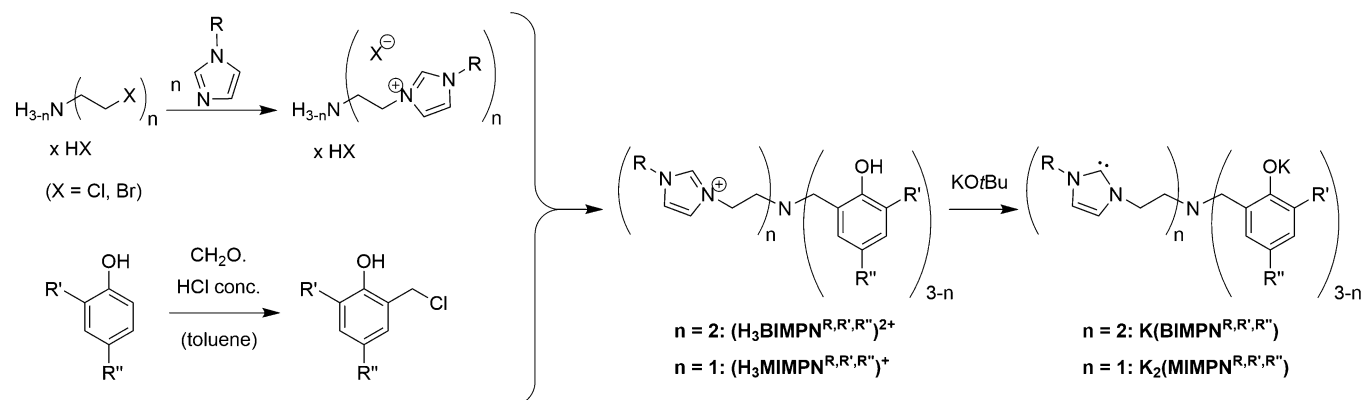
The molecular structures of the cation of (H$_3$-BIMPN^{Mes,Ad,Me})(OTs)$_2$ and of [K$_2$(BIMPN^{Mes,Ad,Me})$_2$(C$_6$H$_6$)] are shown in Figure 1; their structural features are discussed in detail in the Supporting Information.

Coordination to First-Row Transition Metals. The deprotonated ligands react with divalent anhydrous metal chlorides of mid to late first-row transition metals (MnCl$_2$, FeCl$_2$, and CoCl$_2$) to give the complexes **1–12**, which are summarized in Figures 2 and 3.

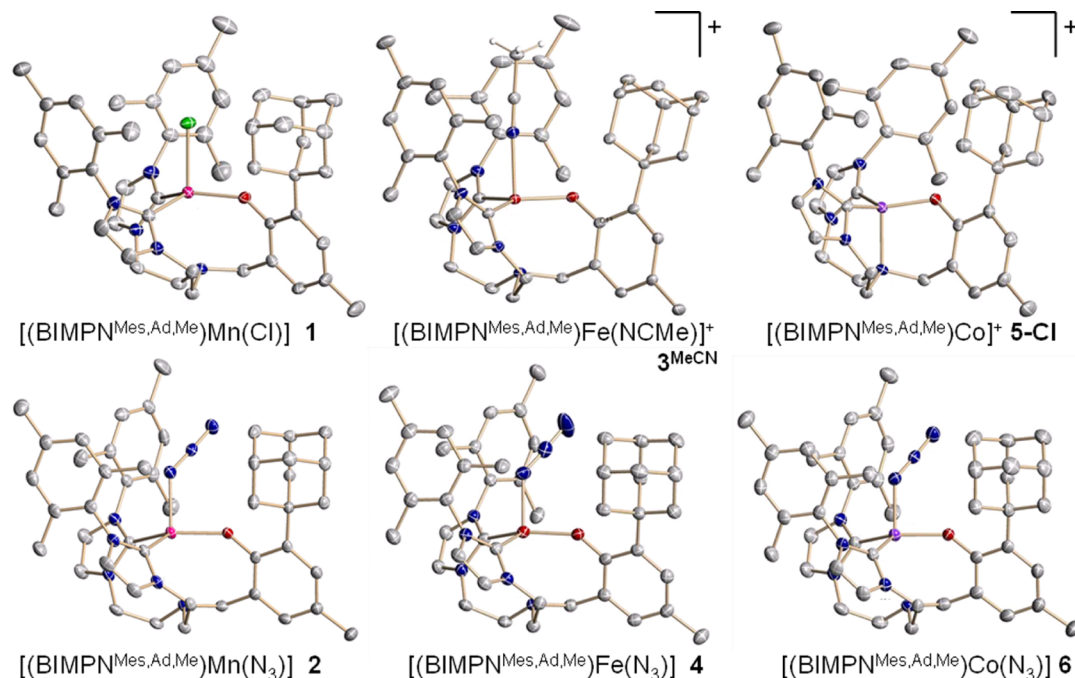**Coordination of the Bis(carbene) Mono(phenolate) Ligand (BIMPN^{Mes,Ad,Me})$^-$ to Mn, Fe, and Co.** Reaction of (BIMPN^{Mes,Ad,Me})$^-$ with 1 equiv of anhydrous manganese chloride in an ether/pyridine mixture (15:1) at room temperature yields the four-coordinate Mn(II) complex [(BIMPN^{Mes,Ad,Me})Mn(Cl)] (**1**) as a white powder in 55% yield. Salt metathesis from chloride to azide affords the colorless complex [(BIMPN^{Mes,Ad,Me})Mn(N$_3$)] (**2**), which is

**Chart 1. Series of Tripodal N-Anchored Ligands from Tris(carbene) (Left) to Tris(phenolate) (Right)**

TIMEN^R | (BIMPN$^{R,R',R''}$)$^-$ | (MIMPN$^{R,R',R''}$)$^{2-}$ | (($^{R',R''}$ArO)$_3$N)$^{3-}$

R = Mes = [structure]   R' = Ad = [structure]   R'' = CH$_3$

Scheme 2. Synthetic Route for K(BIMPN$^{R,R',R''}$) and K$_2$(MIMPN$^{R,R',R''}$)

Figure 1. Molecular structures of the (H$_3$BIMPN^{Mes,Ad,Me})$^{2+}$ cation in crystals of (H$_3$BIMPN^{Mes,Ad,Me})(OTs)$_2$·0.2EtOAc (left) and [K$_2$(BIMPN^{Mes,Ad,Me})$_2$(C$_6$H$_6$)] in crystals of [K$_2$(BIMPN^{Mes,Ad,Me})$_2$(C$_6$H$_6$)]·3Et$_2$O (right). (50% probability ellipsoids; the tosylate counterions, cocrystallized solvent molecules, and—with the exception of the phenol and imidazole H atoms—hydrogen atoms are omitted for clarity; C, gray; H, white; N, blue; O, red; K, light blue).

[(BIMPN^{Mes,Ad,Me})Mn(Cl)] **1**   [(BIMPN^{Mes,Ad,Me})Fe(NCMe)]$^+$ **3^{MeCN}**   [(BIMPN^{Mes,Ad,Me})Co]$^+$ **5-Cl**

[(BIMPN^{Mes,Ad,Me})Mn(N$_3$)] **2**   [(BIMPN^{Mes,Ad,Me})Fe(N$_3$)] **4**   [(BIMPN^{Mes,Ad,Me})Co(N$_3$)] **6**

Figure 2. Molecular structures of complexes [(BIMPN^{Mes,Ad,Me})M(L$_{ax}$)] with M = Mn (L$_{ax}$ = Cl, **1**; N$_3^-$, **2**), M = Fe (L$_{ax}$ = CH$_3$CN, **3^{MeCN}**; N$_3^-$, **4**), and M = Co (L$_{ax}$ = none, **5**; N$_3^-$, **6**) (50% probability ellipsoids; solvent molecules, noncoordinating chlorides, and hydrogen atoms omitted for clarity; C, gray; N, blue; O, red; Mn, magenta; Fe, dark red; Co, purple).
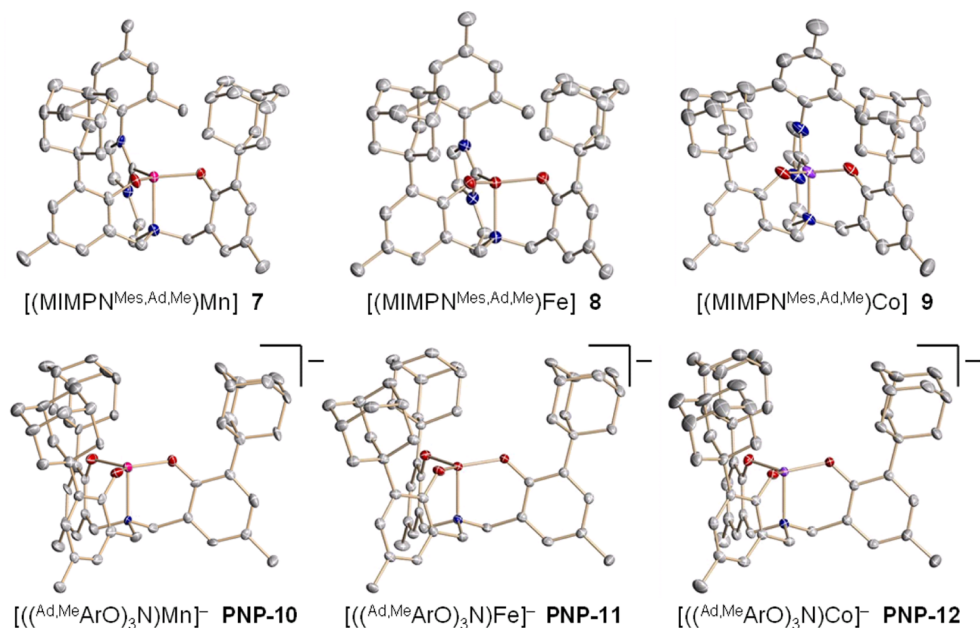
Figure 3. Molecular structures of complexes $[(\text{MIMPN}^{\text{Mes,Ad,Me}})\text{M}]$ with M = Mn (**7**), Fe (**8**), and Co (**9**) and anions of PNP$[((^{\text{Ad,Me}}\text{ArO})_3\text{N})\text{M}]$ with M = Mn (**PNP-10**), Fe (**PNP-11**), and Co (**PNP-12**) (50% probability ellipsoids; solvent molecules, PNP cations (for **PNP-10**−**PNP-12**), and hydrogen atoms omitted for clarity; C, gray; N, blue; O, red; Mn, magenta; Fe, dark red; Co, purple).

Table 1. Selected Bond Distances [Å] and Bond Angles [deg] for $[(\text{BIMPN}^{\text{Mes,Ad,Me}})\text{Mn}^{\text{II}}(\text{Cl})]\cdot0.5\text{pyridine}$ ($1\cdot0.5\text{py}$), $[(\text{BIMPN}^{\text{Mes,Ad,Me}})\text{Fe}^{\text{II}}(\text{NCMe})]\text{Cl}\cdot2\text{MeCN}$ ($3^{\text{MeCN}}\cdot2\text{MeCN}$), $[(\text{BIMPN}^{\text{Mes,Ad,Me}})\text{Co}^{\text{II}}]\text{Cl}\cdot\text{MeCN}$ ($5\text{-Cl}\cdot\text{MeCN}$), $[(\text{MIMPN}^{\text{Mes,Ad,Me}})\text{Mn}^{\text{II}}]\cdot1.5\text{DME}\cdot0.5\text{THF}$ ($7\cdot1.5\text{DME}\cdot0.5\text{THF}$), $[(\text{MIMPN}^{\text{Mes,Ad,Me}})\text{Fe}^{\text{II}}]\cdot1.84\text{THF}\cdot0.46\text{Et}_2\text{O}$ ($8\cdot1.84\text{THF}\cdot0.46\text{Et}_2\text{O}$), $[(\text{MIMPN}^{\text{Mes,Ad,Me}})\text{Co}^{\text{II}}]\cdot2\text{CDCl}_3$ ($9\cdot2\text{CDCl}_3$), PNP$[((^{\text{Ad,Me}}\text{ArO})_3\text{N})\text{Mn}^{\text{II}}]\cdot2.5\text{DME}$ (PNP-10$\cdot2.5\text{DME}$), PNP$[((^{\text{Ad,Me}}\text{ArO})_3\text{N})\text{Fe}^{\text{II}}]\cdot\text{DME}\cdot\text{C}_6\text{H}_6$ (PNP-11$\cdot\text{DME}\cdot\text{C}_6\text{H}_6$), and PNP$[((^{\text{Ad,Me}}\text{ArO})_3\text{N})\text{Co}^{\text{II}}]\cdot\text{DME}$ (PNP-12$\cdot\text{DME}$)[a]

bond/angle	1	3^{MeCN}	5-Cl	7	8	9	PNP-10	PNP-11	PNP-12
$\text{M}\cdots\text{N}_{\text{anchor}}$	2.696	2.461	2.141	2.220	2.166	2.083	2.169	2.112	2.068
$\text{M}-\text{L}_{\text{axial}}$	2.422	2.229							
$\text{M}-\text{C}_{\text{carb.}}$	2.229	2.111	2.024	2.130	2.063	2.009			
$\text{M}-\text{O}$	2.001	1.920	1.875	1.930	1.916	1.882	1.977	1.952	1.919
$\text{N}_{\text{NHC1}}-\text{C}_{\text{carb.}}$	1.361	1.356	1.357	1.350	1.360	1.349			
$\text{N}_{\text{NHC2}}-\text{C}_{\text{carb.}}$	1.363	1.363	1.359	1.360	1.370	1.360			
$\text{N}_{\text{NHC1}}-\text{C}_{\text{carb2}}$	1.383	1.386	1.382	1.388	1.378	1.397			
$\text{C}_{\text{carb2}}-\text{C}_{\text{carb3}}$	1.342	1.348	1.346	1.325	1.347	1.325			
$\text{N}_{\text{NHC2}}-\text{C}_{\text{carb3}}$	1.390	1.387	1.387	1.392	1.386	1.396			
$\text{C}_{\text{ph1}}-\text{O}$	1.319	1.339	1.346	1.334	1.343	1.335	1.342	1.333	1.338
$\text{C}_{\text{ph1}}-\text{C}_{\text{ph2}}$	1.416	1.419	1.413	1.430	1.420	1.426	1.42	1.422	1.421
$\text{C}_{\text{ph2}}-\text{C}_{\text{ph3}}$	1.388	1.398	1.396	1.397	1.397	1.397	1.39	1.384	1.399
$\text{C}_{\text{ph3}}-\text{C}_{\text{ph4}}$	1.390	1.399	1.393	1.390	1.393	1.393	1.40	1.388	1.389
$\text{C}_{\text{ph4}}-\text{C}_{\text{ph5}}$	1.398	1.385	1.384	1.390	1.375	1.397	1.39	1.393	1.397
$\text{C}_{\text{ph5}}-\text{C}_{\text{ph6}}$	1.390	1.395	1.394	1.392	1.401	1.382	1.40	1.396	1.399
$\text{C}_{\text{ph1}}-\text{C}_{\text{ph6}}$	1.433	1.413	1.418	1.416	1.411	1.434	1.42	1.428	1.433
$\text{N}_{\text{anchor}}-\text{M}-\text{L}_{\text{axial}}$	170.25	177.76							
$\text{C}_{\text{carb.}}-\text{M}-\text{L}_{\text{axial}}$	103.72	94.52							
$\text{O}-\text{M}-\text{L}_{\text{axial}}$	92.45	90.45							
$\text{C}_{\text{carb.}}-\text{M}-\text{C}'_{\text{carb.}}$	109.03	120.82	117.40						
	130.70	117.61	112.72	115.7	125.2	129.5			
$\text{C}_{\text{carb.}}-\text{M}-\text{O}$	111.60	120.66	124.65	132.1	115.1	114.0			
							128.7	118.43	117.81
$\text{O}-\text{M}-\text{O}'$				111.2	117.3	111.9	109.9	106.84	116.60
							120.6	132.63	120.70
$\text{N}_{\text{NHC1}}-\text{C}_{\text{carb.}}-\text{N}_{\text{NHC2}}$	103.3	103.2	103.62	104.4	103.3	104.5			
d_{oop}	0.362	0.113	−0.262	−0.109	−0.175	−0.238	−0.107	−0.161	−0.247

[a]See Chart 2 for atom labeling. Given are the mean values for each bond or angle type; a full list of metric parameters and e.s.d.'s are listed in Tables S7−S12 (Supporting Information).

Table 2. Selected Bond Distances [Å] and Bond Angles [deg] for the Ligand Structures (H₃BIMPN^{Mes,Ad,Me})(OTs)₂·0.2EtOAc (A) and [K₂(BIMPN^{Mes,Ad,Me})₂(C₆H₆)]·3Et₂O·0.5C₆H₆ (B and B′) and the Azide Complexes [(BIMPN^{Mes,Ad,Me})Mn^{II}(N₃)]· 3C₆H₆ (2·3C₆H₆), [(BIMPN^{Mes,Ad,Me})Fe^{II}(N₃)]·1.894Et₂O·0.606DMF (4·1.984Et₂O·0.606DMF), and [(BIMPN^{Mes,Ad,Me})Co^{II}(N₃)]·2THF·0.5C₆H₆ (6·2THF·0.5C₆H₆) and, for Comparison, TIMEN Azide Complexes [(TIMEN^{Xyl})Mn(N₃)]BPh₄·MeCN (C·MeCN), [(TIMEN^{Mes})Fe(N₃)]BPh₄·2.5THF (D·2.5THF), and [(TIMEN^{Xyl})Co(N₃)]BPh₄·MeCN (E·MeCN)[a]

bond/angle	A	B	B′	2	4	6	C	D	E
M···N_anchor				2.626	2.591	2.659	3.137	3.243	3.213
M−L_axial				2.125	2.062	2.039	2.031	1.947	1.938
M−C_carb.				2.204	2.123	2.071	2.179	2.108	2.039
M−O				2.007	1.940	1.932			
Nα−Nβ				1.190	1.175	1.188	1.184	1.182	1.161
Nβ−Nγ				1.168	1.160	1.164	1.160	1.156	1.169
N_NHC1−C_carb.	1.328	1.365	1.368	1.359	1.359	1.356	1.361	1.362	1.357
N_NHC2−C_carb.	1.335	1.370	1.373	1.356	1.364	1.361	1.370	1.365	1.364
N_NHC1−C_carb2	1.380	1.385	1.383	1.383	1.384	1.378	1.387	1.383	1.384
C_carb2−C_carb3	1.347	1.341	1.345	1.340	1.343	1.339	1.339	1.339	1.337
N_NHC2−C_carb3	1.335	1.390	1.385	1.386	1.386	1.384	1.388	1.386	1.383
C_ph1−O	1.369	1.313	1.315	1.324	1.327	1.319			
C_ph1−C_ph2	1.412	1.441	1.426	1.402	1.412	1.411			
C_ph2−C_ph3	1.400	1.392	1.390	1.390	1.393	1.389			
C_ph3−C_ph4	1.391	1.376	1.389	1.383	1.384	1.381			
C_ph4−C_ph5	1.389	1.399	1.396	1.394	1.395	1.392			
C_ph5−C_ph6	1.390	1.391	1.395	1.390	1.394	1.391			
C_ph1−C_ph6	1.406	1.446	1.449	1.427	1.429	1.428			
N_anchor−M−L_axial				168.71	170.2	168.9	175.4	177.5	174.3
C_carb.−M−L_axial				102.57	101.3	103.67	103.9	105.2	104.8
O−M−L_axial				91.26	92.75	89.93			
M−Nα−Nβ				130.3	134.9	128.3	167.5	174.5	166.3
Nα−Nβ−Nγ				177.9	177.8	177.1	179.3	179.6	178.3
							119.15	115.3	118.8
C_carb.−M−C′_carb.				107.90	107.8	106.95	110.97	112.5	111.9
							113.26	112.1	110.5
C_carb.−M−O				134.27	138.33	134.03			
				111.63	108.30	112.31			
N_NHC1−C_carb.−N_NHC2	108.2	101.6	101.6	103.1	102.9	103.0	103.3	102.9	103.4
d_oop				0.301	0.271	0.297	0.521	0.554	0.520

[a]See Chart 2 for atom labeling. Given are the mean values for each bond or angle type, as well as average values for the two independent molecules of the [(BIMPN^{Mes,Ad,Me})M^{II}(N₃)] complexes; all single values and their e.s.d.'s are listed in Tables S7−S10 (Supporting Information).

Chart 2. Schematic Drawing of Complexes with Atom Labels Used in Tables 1 and 2

n	ligand
3	TIMEN^R
2	(BIMPN^{R,R′,R″})⁻
1	(MIMPN^{R,R′,R″})²⁻
0	((^{Ad,Me}ArO)₃N)³⁻
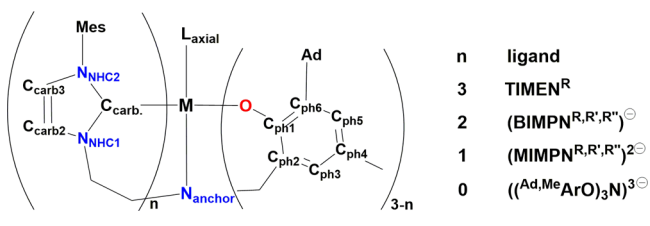
easily identified by the intense and very characteristic $\tilde{\nu}$ (N₃) IR vibrational bands (in KBr: 2077 and 2056 cm⁻¹). Both Mn^{II} complexes are NMR-silent. The UV/vis-spectra of both complexes feature bands with maxima at 257 and 309 nm of similar intensity (ε = 11 300 and 5750 M⁻¹ cm⁻¹ for **1**, 14 900 and 7400 M⁻¹ cm⁻¹ for **2**), which we tentatively assign to a π−π^* transition in the phenolate and a charge-transfer (CT) transition, respectively.[26]

A yellow powder of [(BIMPN^{Mes,Ad,Me})Fe]Cl (**3**) was obtained in a procedure analogous to that used for **1** in 80% yield. The paramagnetic ¹H NMR spectra of **3** (in MeCN-d_3,

CDCl₃, or DMSO-d_6) feature signals ranging from 55 to −10 ppm, some of which are strongly broadened and, in part, overlapping with each other, thus, preventing unequivocal signal assignment and integration. However, the characteristic spectra with the two comparatively sharp peaks around 50 ppm with relative intensities of 3:1 allow for the identification and determination of the purity of the complex. While the solid-state molecular structure derived by X-ray crystallography exhibits C_1 symmetry (*vide infra*), with two complexes related by an inversion center in the unit cell, the ¹H NMR spectra in polar solvents suggest a dynamic behavior in solution, resulting in C_s symmetry on the NMR time scale. The structure of the complex in solution also appears to vary depending on the solvent's ability to coordinate the metal and solvate the chloride counterion, as is indicated by the markedly different signal distribution of the ¹H NMR spectrum in THF-d_8 compared to MeCN-d_3, CDCl₃, or DMSO-d_6.

Salt metathesis from chloride to azide affords [(BIMPN^{Mes,Ad,Me})Fe(N₃)] (**4**), which, similar to **2**, is identified by the intense and characteristic $\tilde{\nu}$ (N₃) IR vibrational bands (in KBr: 2086, 2054, and 2001 cm⁻¹).[27] The ¹H NMR spectra of **4** in polar solvents, such as CDCl₃ and MeCN-d_3, are practically

identical to those of **3**, whereas, in THF-d_8, the signals of both complexes differ significantly, clearly indicating that the azide and chloride counterions are coordinated only in THF solutions.

The green cobalt complex [(BIMPN^{Mes,Ad,Me})Co]Cl (**5-Cl**) was obtained by stirring an excess of K(BIMPN^{Mes,Ad,Me}) and CoCl$_2$ in benzene for at least 24 h, during which time the crude, green complex precipitates. Impurities of KCl can gradually be reduced by repeatedly redissolving the crude material in MeCN or CH$_2$Cl$_2$, followed by filtration through Celite and evaporation. The difficulty in removing KCl from the bulk material of all (BIMPN^{Mes,Ad,Me})$^-$ chloride complexes (**1**, **3**, and **5-Cl**) suggests some interaction with the complex, e.g., coordination of K$^+$ to the phenol oxygens (see below).

Anion exchange of Cl$^-$ to PF$_6^-$ or N$_3^-$ allows for a more straightforward workup to obtain the analytically pure complexes [(BIMPN^{Mes,Ad,Me})Co]PF$_6$ (**5-PF$_6$**) and [(BIMPN^{Mes,Ad,Me})Co(N$_3$)] (**6**) that are easily identifiable by their characteristic strong IR bands (in KBr: 843 cm^{-1} for PF$_6^-$, 2081, 2044, and 1999 cm^{-1} for the coordinated azide in **6**).[27]

When dissolved in MeCN, the blue azide complex **6** changes its color to the same green color as the azide-free complexes [(BIMPN^{Mes,Ad,Me})Co^{II}]$^+$ dissolved in MeCN. Accordingly, the ^{1}H NMR spectra of the Co^{II}-complexes **5-Cl**, **5-PF$_6$**, and **6** in MeCN-d_3 and CDCl$_3$ feature the same signals (within the error margins for highly temperature-dependent paramagnetic NMR shifts). In THF-d_8, the signal distribution of **5-PF$_6$** remains the same, whereas **6** gives rise to a very different spectrum with more signals. All of these observations lead to the conclusion that—in MeCN and chloroform solutions—the divalent Fe and Co complexes [(BIMPN^{Mes,Ad,Me})M]$^+$ (M = Fe, Co) exist in the monocationic form with the anion *not* coordinated, but solvated, whereas, in THF solution, the Cl$^-$ or N$_3^-$ anions coordinate to the metal centers.

In addition to the absorption bands observed for the Mn(II) complexes, the UV/vis spectra of the (BIMPN^{Mes,Ad,Me})$^-$ cobalt complexes exhibit metal-centered Laporte and spin-forbidden d–d transitions of low intensity.

Tables 1 and 2 summarize bond lengths and angles of all new complexes, along with selected TIMEN^R azide complexes for comparison, as well as the out-of-plane shift d_{oop}, which is defined as the distance of the metal center from the least-squares plane defined by the three coordinating atoms of the tripodal ligand, i.e., the carbene carbon and phenolate oxygen atoms. In general, the Mn–C$_{carb}$ bond distances observed in complexes **1**, **2**, and **7** (2.130(5)−2.230(3) Å) compare well with those in the literature reported Mn–NHC complexes (2.175(3)−2.277(4) Å).[28] Similarly, the Fe–C$_{carb}$ bond lengths seen in complexes **3^{MeCN}**, **4**, and **8** (2.063(4)−2.144(3) Å) fall within the range as those observed for literature Fe–NHC complexes (2.072(3)−2.166(10) Å).[29]

Crystals of **1** suitable for X-ray crystal structure determination were obtained as colorless prisms by slow diethyl ether diffusion into a pyridine solution of the complex. The molecular structure of this manganese complex exhibits C_1 symmetry. The central manganese(II) ion is coordinated by the NHC carbenes, phenolate oxygen, and the chloride in a distorted trigonal-pyramidal geometry. The manganese is located above the plane of the three donor atoms O1, C3, and C8 (toward Cl1), as is indicated by the corresponding d_{oop} of 0.362(2) Å. Notably, a non-coordinated pyridine molecule is situated between the adamantyl and one of the mesityl substituents, with one C–H bond pointing toward the Mn–Cl bond (at a

distance of ca. 3 Å; see Figure 4). This observation demonstrates the intended steric flexibility of the (BIMPN$^{R,R',R''}$)$^-$ ligand to provide side access for organic substrates to the reactive center.
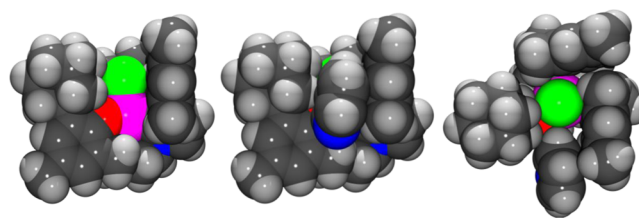
Figure 4. Space-filling representations of the molecular structure of **1** in crystals of [(BIMPN^{Mes,Ad,Me})Mn^{II}Cl]·0.5pyridine; side view with and without the pyridine molecule situated between two ligand arms (left and middle) and top view (right) down the Mn–Cl axis; C, gray; H, white; N, blue; O, red; Cl, green; Mn, magenta.

Nearly colorless prismatic crystals of **3** suitable for X-ray crystallography were obtained by slow diethyl ether diffusion into an acetonitrile solution of the complex. The molecular and crystal structure reveals an acetonitrile molecule bound axially to the iron center (**3^{MeCN}**). The coordination geometry at the iron center can be described as nearly trigonal-bipyramidal, with the iron atom positioned 0.113(1) Å above the plane defined by the two carbene carbons and the oxygen atom and a near linear angle between the anchoring and acetonitrile nitrogens ((N$_{MeCN}$–Fe–N$_{anchor}$) = 177.76(5)°). An Fe–N$_{anchor}$ distance of 2.462(2) Å is indicative of a weak bonding interaction between the nitrogen anchor and the iron center.

Single crystals of **5-Cl** were also obtained from an acetonitrile solution.[30] While the manganese center in **1** contains an axially coordinated chlorido ligand and the axial position in the corresponding iron complex **3^{MeCN}** is occupied by an acetonitrile solvent molecule, the cobalt center in **5-Cl** is coordinated solely by the chelating (BIMPN^{Mes,Ad,Me})$^-$ ligand in a distorted trigonal-pyramidal fashion. Thus, the cobalt ion prefers binding to the nitrogen anchor over the chloride counterion or an acetonitrile solvent molecule. Consequently, going from Mn to Fe to Co, the out-of-plane shift d_{oop} above the plane decreases from 0.362(2) Å (**1**) to 0.113(1) Å (**3^{MeCN}**) to −0.261(1) Å (**5-Cl**) below the plane toward the N-anchor. Accordingly, d(M–N$_{anchor}$) decreases from 2.695(2) Å (no interaction in **1**) to 2.461(2) Å (weak interaction in **3^{MeCN}**), to 2.141(2) Å (cobalt bound to N$_{anchor}$ in **5-Cl**).

In the molecular structures of the azide complexes **2**, **4**, and **6**, the metal center is coordinated in a trigonal-pyramidal fashion, with the carbene and phenolate C and O donor atoms of the (BIMPN^{Mes,Ad,Me})$^-$ ligand occupying the equatorial positions while the azide resides in the axial position. For all three azide complexes, two crystallographically independent molecules are present within the unit cell. Table 2 summarizes the complex metrics of one representative only; parameters for each independent molecule are listed in Tables S7−S10 (Supporting Information).

Notably, the azide is coordinated in its preferred bent coordination mode (e.g., in **4**: Fe1–N6–N7 = 134.9(2)°) in contrast to the azide ligands in the corresponding TIMEN^{Mes} complexes, which are forced into linear coordination by the cylindrical cavity formed by the mesityl substituents of the NHCs ([(TIMEN^{Mes})Fe(N$_3$)]$^+$: 174.5(2)°).[17] Therefore, even with the bulky adamantyl substituent on the phenol, the steric

pressure at the metal center has already been decreased compared to that in the TIMEN^R-complexes by the substitution of one of the NHCs with a phenol arm. The azide protrudes into the gap between the phenolate and one of the carbene arms thus widening the corresponding angles ($C_{Carb.}$−M−O) to over 130° (see Figure 5).
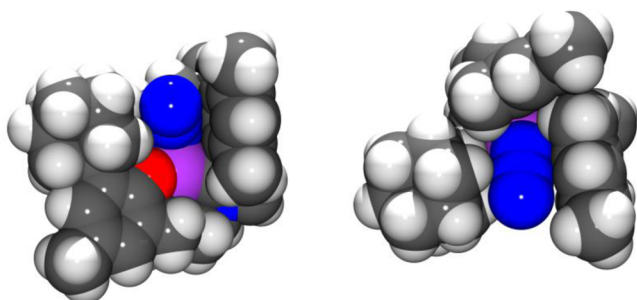
Figure 5. Space-filling representations of the molecular structure of **4** in crystals of [(BIMPN^{Mes,Ad,Me})Fe^{II}N$_3$]·1.894Et$_2$O·0.606DMF; side view (left) and top view (right), along the N$_{azide}$−Fe−N$_{anchor}$ axis; C, gray; H, white; N, blue; O, red; Co, purple.

The azide's linear coordination mode in the [(TIMEN^{Mes})-M(N$_3$)]$^+$ complexes (M = Mn, Fe, Co) is accompanied by an M−Nα bond that is approximately 0.1 Å shorter than the corresponding bond in the (BIMPN$^{R,R',R''}$)$^-$ azide complex of the same metal. Additionally, the [(TIMEN^{Mes})M(N$_3$)]$^+$ complexes exhibit a larger displacement of the metal ions above the plane of the three coordinating carbenes of the TIMEN^{Mes} ligand (d_{oop}), all of which indicates increased double bond character between the metal center and the coordinating Nα nitrogen of the azide ligand.

Coordination of the Mono(carbene) Bis(phenolate) Ligand (MIMPN^{Mes,Ad,Me})$^{2-}$ to Mn, Fe, and Co. Under an inert gas atmosphere, the reaction of the (MIMPN^{Mes,Ad,Me})$^{2-}$ ligand with 0.7 equiv of anhydrous manganese, ferrous, or cobalt dichloride yields [(MIMPN^{Mes,Ad,Me})Mn] (**7**) and [(MIMPN^{Mes,Ad,Me})Fe] (**8**) as colorless and [(MIMPN^{Mes,Ad,Me})Co] (**9**) as green solids in approximately 60% isolated yields.

While complex **7** is ^{1}H NMR-silent, the ^{1}H NMR spectrum of **8** (THF-d_8) features five paramagnetically broadened and shifted signals from 40 to −7 ppm with half-widths ranging from 200 to 340 Hz. In contrast, the spectrum of **9** (CDCl$_3$) features 10 signals from 45 to −5 ppm. The less detailed spectrum of **8** prevents a definitive signal assignment but is characteristic of the spectroscopically and analytically pure complex.

The molecular and crystal structures of all three [(MIMPN^{Mes,Ad,Me})M^{II}] (M = Mn, Fe, Co) complexes, derived by single-crystal X-ray crystallography, feature a metal center coordinated in a trigonal-pyramidal fashion solely by the chelating (MIMPN^{Mes,Ad,Me})$^{2-}$ ligand. The metal center of the neutral complex is located below the plane defined by the carbene carbon and two phenolate oxygen atoms (negative d_{oop}), demonstrating that binding to the nitrogen anchor seems favored over binding to an axial ligand *trans* to the N anchor, such as available halide anions or coordinating solvent molecules. As the ionic radius of the divalent ion decreases from Mn to Co, all four M−L bond distances decrease and the out-of-plane shift of the metal ions increases, moving the metal

atoms closer to the ligand N-anchor (d_{oop} = −0.109, −0.175, and −0.238 Å for **7**, **8**, and **9**).

Coordination of the Tris(phenolate) Ligand ((^{Ad,Me}ArO)$_3$N)$^{3-}$ to Mn, Fe, and Co. Reaction of Na$_3$-((^{Ad,Me}ArO)$_3$N) with anhydrous manganese chloride in an acetonitrile/DME mixture (9:1) in the presence of [PNP]Cl (PNP = PNP$^+$ = bis(triphenylphosphine)iminium) generates ^{1}H NMR-silent, yellow [PNP][((^{Ad,Me}ArO)$_3$N)Mn] (**PNP-10**) in 75% isolated yield.

Analogously, reaction of Na$_3$((^{Ad,Me}ArO)$_3$N) with 1 equiv of anhydrous ferrous chloride in a 1:1 mixture of THF and acetonitrile at room temperature yields the four coordinate Fe(II) complex Na[((^{Ad,Me}ArO)$_3$N)Fe] (**Na-11**) as a colorless solid in 94% yield. Exposure to oxygen or chloroform yields the neutral, dark brown, air-stable Fe(III) complex.[31] The paramagnetic ^{1}H NMR spectrum (THF-d_8) of **Na-11** features seven signals between 30 and 0.5 ppm, consistent with the expected C_3 symmetry on the NMR time scale. Due to paramagnetic broadening, however, the unambiguous assignment of these characteristic signals is not possible.

The addition of anhydrous CoCl$_2$, dissolved in acetonitrile, to Na$_3$((^{Ad,Me}ArO)$_3$N) at room temperature yields a dark blue solution. After filtration, removal of the solvent, and recrystallization from THF/hexane, dark blue crystals of Na[((^{Ad,Me}ArO)$_3$N)Co]·2THF (**Na-12·2THF**) were obtained in 68% yield. The ^{1}H NMR spectrum (MeCN-d_3) shows six paramagnetic signals between 39 and −3 ppm as well as resonances from cocrystallized THF. Considering the likely C_3 symmetry in solution, the signal at 8.68 ppm, which is considerably broader than the other five signals (220 Hz compared to 30 Hz), may arise from an accidental degeneracy of two resonances. In spectra recorded in THF-d_8, this signal is more resolved, and hence, two overlapping signals at 9.40 ppm (broad, half-width 300 Hz) and 8.60 ppm (half-width 90 Hz) are detectable. The chemical shifts of the other signals are very similar to those of the spectrum in acetonitrile. Although an unambiguous signal assignment of the paramagnetic spectra is not possible, the ^{1}H NMR spectra are characteristic of the synthesized compounds and provide useful information regarding the compounds' identity and purity.

Single crystals of **11** and **12** were obtained after cation exchange from a sodium counterion to the bis(triphenyl-phosphine)iminium (PNP$^+$) (**PNP-10**, **PNP-12**). In all three molecular structures, the coordination of the chelating tris(phenolate) at the central metal is best described as distorted trigonal-pyramidal.

As in the (MIMPN^{Mes,Ad,Me})$^{2-}$ system, all four bond distances to the metal center decrease in going from Mn (**PNP-10**) to Co (**PNP-12**), with the divalent metal ion moving more and more below the phenolate oxygen plane toward the anchoring N atom. For a given metal, the M−N$_{anchor}$ bond distance is shorter, and the average M−O bond length is longer in the tris(phenolate) system than in complexes with the (MIMPN^{Mes,Ad,Me})$^{2-}$ ligand. This trend persists even when the structure of the (BIMPN^{Mes,Ad,Me})$^-$ complex **5-Cl** is taken into account.[32] For the cobalt series **5-Cl**, **9**, and **PNP-12**, the following trend applies: the more phenolates, the longer the average M−O bond, and the shorter the M−N$_{anchor}$.

Interestingly, while the phenolate ligand is known to be redox-active, and occasionally exhibits radical character,[33−35] the divalent complexes presented herein exhibit full aromaticity of the phenolate chelating arms. None of the C−C bonds of the phenolate ring in either the potassium salt of the free ligand

(structure of K(BIMPN^{Mes,Ad,Me}), *vide supra*) or the 12 complexes **1** to **PNP-12** differ significantly from 1.39 Å (see Tables S11 and S12 in the Supporting Information for full lists of relevant metric parameters). The only exceptions are the two bonds in the phenolate ring with adjacent carbon atoms bearing substituents (the methylene bridge to the N-anchor, the phenolate oxygen or the adamantyl substituent). Apparently, the steric strain introduced by these substituents lengthens these bonds by about 0.02−0.03 Å.[36]

The space-filling representations of the three cobalt complexes **5-Cl**, **9**, and **PNP-12** (Figure 6) reveal that
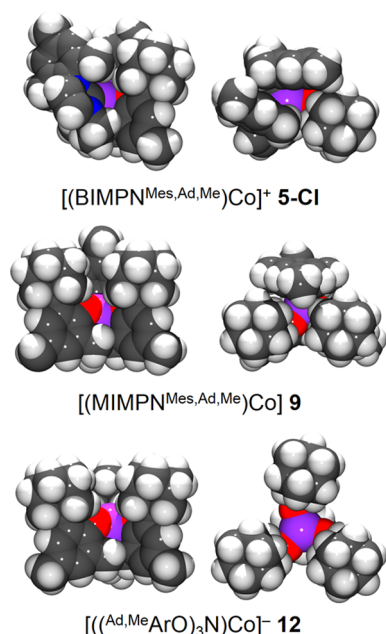
Figure 6. Space-filling representations of the three new Co(II) complexes, each with side view (left) and top view (right) along the M−N$_{anchor}$ axis; C, gray; H, white; N, blue; O, red; Co, purple.

replacement of NHCs with phenolates reduces the steric bulk as desired. However, in the absence of an axial ligand, the mesityl substituents on the remaining NHC rings seem to bend down and obstruct axial access to the metal center. The molecular structures of the azide complexes **2**, **4**, and **6**, as well as [(BIMPN^{Mes,Ad,Me})Mn(Cl)] (**1**) with its intercalated pyridine, prove, however, that the new ligands are flexible enough to enable side access for organic substrates, a feature that is not present in complexes of the tris(carbene) TIMEN^R system.

Magnetization Measurements. Variable-temperature SQUID magnetization measurements (2−300 K) confirm *high-spin* ground states for all complexes and show remarkably similar temperature dependencies of the magnetic moment for complexes of the same metal ion across the ligand series (Figure 7, Table 3): At room temperature, manganese complexes **1**, **7**, and **PNP-10** possess magnetic moments, μ_{eff}, between 5.8 and 6.0 μ_B ($S = 5/2$ ground state) that decrease negligibly with decreasing temperature down to 10 K. From this temperature on, μ_{eff} drops to values between 5.1 and 5.3 μ_B at 2 K. Likewise, iron complexes **8** and **Na-11** possess room-temperature magnetic moments of 5.04 and 4.92 μ_B ($S = 2$ ground state), which decrease slightly with decreasing temperature (4.89 and 4.70 μ_B at 15 K) and result in low-temperature values of 3.70 and 3.59 μ_B at 2 K. While the μ_{eff} value of the
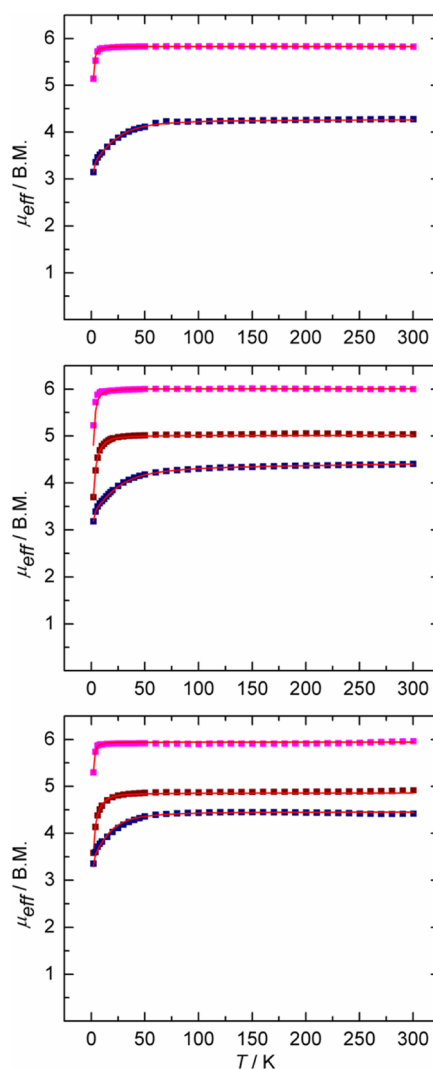
Figure 7. Temperature-dependent SQUID magnetization data (1 T) for complexes of (BIMPN^{Mes,Ad,Me})$^-$ (top), (MIMPN^{Mes,Ad,Me})$^-$ (middle), and ((^{Ad,Me}ArO$_3$)N)$^{3-}$ (bottom). Magnetic moment (μ_{eff}) plotted vs temperature (T). Magenta: Mn complexes **1**, **7**, and **10**; brown: Fe complexes **8** and **Na-11**; blue: Co complexes **5-PF$_6$**, **9**, and **Na-12**; red lines: simulation. Data were corrected for underlying diamagnetism. Reproducibility was confirmed by measuring multiple independently synthesized samples.

manganese and iron complexes at room temperature are found near the spin-only values (5.92 μ_B for $S = 5/2$, 4.90 μ_B for $S = 2$), the magnetic moments of the cobalt complexes are reproducibly around 4.3−4.4 μ_B and, thus, significantly larger than the spin-only value for an $S = 3/2$ system (3.87 μ_B), suggesting a considerable contribution from spin−orbit coupling. The magnetic moments of **5-PF$_6$**, **9**, and **Na-12** decrease slightly with decreasing temperature until they start dropping at approximately 70 K to values between 3.1 and 3.4 μ_B at 2 K. Simulations confirm a trend for the zero-field-splitting parameter D that is already evident by visual inspection of the curve progressions, namely, that $|D(Mn)| < |D(Fe)| \ll |D(Co)|$. Azide complexes **2** and **6** display virtually the same μ_{eff} at RT as their analogous complexes **1** and **5-PF$_6$** with chloride and PF$_6^-$ counterions; however, the μ_{eff} remains high for a larger temperature range, indicative of considerably smaller zero-field splittings (see Figures S11 and S25 and Table S1, Supporting Information).

H

dx.doi.org/10.1021/ic4024053 | *Inorg. Chem.* XXXX, XXX, XXX−XXX

Table 3. Effective Magnetic Moments μ_{eff} at Room Temperature Derived from the Magnetization Measurements and the Corresponding Parameters Used for Simulation of the Experimental Data

complex		μ_{eff} (RT) [μ_B]	g value	$|D|$ [cm^{-1}]	$|E/D|$
[(BIMPN^{Mes,Ad,Me})MnCl]	(1)	5.82	1.970	0.426	0.000
[(BIMPN^{Mes,Ad,Me})Mn(N$_3$)]	(2)	5.78	1.958	0.365	0.019
[(BIMPN^{Mes,Ad,Me})Co]PF$_6$	(5-PF$_6$)	4.28	2.202	26.837	0.000
[(BIMPN^{Mes,Ad,Me})Co(N$_3$)]	(6)	4.42	2.266	7.086	0.305
[(MIMPN^{Mes,Ad,Me})Mn]	(7)	6.00	2.030	2.041	0.025
[(MIMPN^{Mes,Ad,Me})Fe]	(8)	5.04	2.045	4.359	0.333
[(MIMPN^{Mes,Ad,Me})Co]	(9)	4.40	2.234	29.720	0.000
PNP[((^{Ad,Me}ArO)$_3$N)Mn]	(PNP-10)	5.96	2.008	0.093	0.002
Na[((^{Ad,Me}ArO)$_3$N)Fe]	(Na-11)	4.92	1.982	4.552	0.333
Na(THF)$_2$[((^{Ad,Me}ArO)$_3$N)Co]	(Na-12·2THF)	4.42	2.302	20.395	0.000

Table 4. Mössbauer Parameters for All Iron Complexes Discussed Herein

complex		δ [mm·s^{-1}]	ΔE_Q [mm·s^{-1}]	Γ_{fwhm} [mm·s^{-1}]
[(TIMEN^{Mes})Fe^{II}]OTf$_2$[39]		0.59(1)	1.02(1)	0.40(1)
[(BIMPN^{Mes,Ad,Me})Fe^{II}]Cl	(3)	0.68(1)	3.28(1)	0.27(1)
[(MIMPN^{Mes,Ad,Me})Fe^{II}]	(8)	0.81(1)	3.09(1)	0.38(1)
Na[((^{Ad,Me}ArO)$_3$N)Fe^{II}]	(Na-11)	1.06(1)	2.08(1)	0.37(1)
PNP[((^{Ad,Me}ArO)$_3$N)Fe^{II}]	(PNP-11)	1.04(1)	2.24(1)	0.30(1)
[(TIMEN^{Mes})Fe^{II}(N$_3$)]BPh$_4$[17]		0.687(1)	2.267(3)	0.48(1)
[(BIMPN^{Mes,Ad,Me})Fe^{II}(N$_3$)]	(4)	0.83(1)	3.24(1)	0.31(1)

Mössbauer Spectroscopy. The zero-field ^{57}Fe Mössbauer spectra of all new iron complexes presented herein feature doublets with isomer shifts, δ, in agreement with *high-spin* iron(II) complexes (see Table 4).[37,38] The isomer shifts δ of the respective iron(II) complexes increase stepwise as carbenes are substituted by phenolates in the ligand series from the tris(carbene) all the way to the tris(phenolate) ligand derivative. This is most evident when comparing the complexes without additional axial ligands, [(TIMEN^{Mes})Fe]OTf$_2$ (δ = 0.59 mm·s^{-1}),[39] **3**, **8**, and **Na-11** (δ = 1.06(1) mm·s^{-1}),[39] where each phenolate arm adds 0.1−0.2 mm·s^{-1} to the observed isomer shift; the same is observed for the two azide complexes [(TIMEN^{Mes})Fe(N$_3$)]BPh$_4$ and [(BIMPN^{Mes,Ad,Me})Fe^{II}(N$_3$)] (**4**). This trend is accounted for by the different electronic properties of the NHC and phenolate ligands. While the σ-donating NHCs also engage in metal-to-ligand π-backbonding,[40] the phenolates are σ and π donors. This leads to a higher d-electron density at the metal, which, in turn, increases the shielding of the s orbitals vs the nuclear charge. The s orbitals expand in volume and the electron density within the iron nucleus is effectively lowered, which increases the isomer shifts, δ, in ^{57}Fe Mössbauer spectroscopy.

For a variety of simple, tetrahedral bis(carbene) dihalide Fe(II) complexes, isomer shifts and quadrupole splittings of δ = 0.70−0.81 mm·s^{-1} and ΔE_Q = 3.67−4.03 mm·s^{-1} have been reported.[29i,j] While these Mössbauer parameters appear to be characteristic for four-coordinate, divalent iron−carbene species, the complexes investigated in this study show significantly different values, ranging from δ = 0.59−1.06 mm·s^{-1} and ΔE_Q = 1.02−3.28 mm·s^{-1}. This is most likely due to the considerably different coordination geometry and ligand environment.

It is less obvious to formulate a trend for the observed quadrupole splittings, ΔE_Q, in the series of high-spin Fe complexes measured and presented herein. In general, the quadrupole splitting of the (BIMPN^{Mes,Ad,Me})$^-$ Fe(II) complexes is considerably larger than that of the corresponding

TIMEN^{Mes} complexes, which may be accounted for by the reduced symmetry at the iron center. This ligand contribution to the total EFG results in a less symmetric distribution of the electron density in the mixed NHC/phenolate complexes (the formal *valence contribution* to the EFG is the same for all high-spin Fe(II) complexes presented herein). Accordingly, the ΔE_Q of **8** is similar compared to **3**, since the ligand field is comparable in symmetry. In contrast, the (idealized) C_3 symmetrical tris(phenolate) complex **11** gives rise to an "in-between" quadrupole splitting, independent of the counterion of the complex. The crystal structure of **PNP-11**, with a PNP$^+$ cation, reveals that the C_3 symmetry is somewhat distorted by intercalation of the cation's phenyl substituents (in the solid state). A similar distortion may be caused by the sodium cations binding to the phenyl moieties in complexes **Na-11**. Although single-crystals of **Na-11** with a sodium cation have not been obtained, this kind of distortion has been observed in the very closely related cobalt complex, namely, Na[(^{tBu,tBu}ArO)$_3$N)Co] (see the Supporting Information for synthesis and XRD studies), where the sodium cation is bound to two of the three aryloxides just above the Co site. This significantly reduces the complexes' C_3 symmetry.[41] However, the same compound, crystallized with the bulky PNP$^+$ cation, does not have direct interactions between the cation and the aryloxide oxygens. The two different resultant complex symmetries are also directly observable in frozen solution at low temperature by X-band EPR spectroscopy; see Figure 8. The EPR spectra of the S = 3/2 Co(II) is very different depending on the solvent: If the compound Na[(^{tBu,tBu}ArO)$_3$N)Co]·THF is dissolved in polar CH$_3$CN, the result is a well-defined *axial* spectrum, showing hyperfine coupling to ^{59}Co (I = 7/2) only in the parallel component. If the same compound is dissolved in nonpolar benzene, a *rhombic* spectrum is obtained with the same average g-values but with pronounced splitting between the two perpendicular components, which is due to rhombic zero-field splitting and/or splitting in the perpendicular g-values.[42] We explain the EPR spectral change from axial to
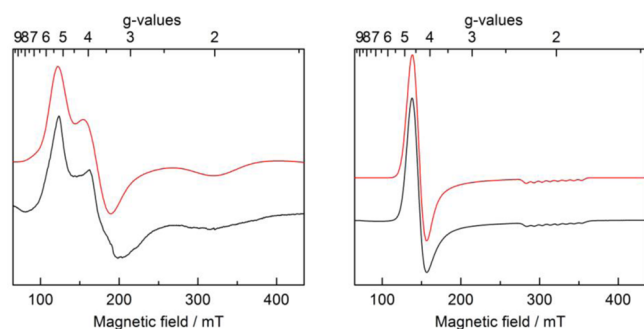
Figure 8. Left graph (rhombic): The black trace is the experimental X-band EPR spectrum (12 K, ν = 8.99756 GHz, power = 0.249 mW, modulation amplitude = 0.25 mT) of $Na[((^{tBu,tBu}ArO)_3N)Co^{II}]\cdot 2THF$ dissolved in a pure benzene glass. The red trace is the simulation using a rhombic $S = 3/2$ spin Hamiltonian with a large zero-field-splitting parameter: $D \gg h\nu$. The simulation parameters used were: $D = -10$ cm^{-1}, $E/D = -0.08$, g_z (=$g_\parallel$) = 2.02, g_y = 2.10 and g_x = 2.33, $A_\parallel$ = 4 · 10^{-4} cm^{-1} (hyperfine coupling to ^{59}Co, I = 7/2), line width = 27 mT, but only the g_z value is determined independently, since both a nonzero rhombic zero-field-splitting parameter, E, and nonequal $g_\perp$ values will split the perpendicular line at g = 4.3. Right graph (axial): The black trace is the experimental X-band EPR spectrum (13 K, ν = 8.99479 GHz, power = 0.249 mW, modulation amplitude = 0.25 mT) of exactly the same salt: $Na[((^{tBu,tBu}ArO)_3N)Co^{II}]\cdot 2THF$, but this time dissolved in a pure acetonitrile glass. The red trace is the simulation using an axial $S = 3/2$ spin Hamiltonian with a large zero-field-splitting parameter: $D \gg h\nu$. The simulation parameters used were: $D = -10$ cm^{-1}, $E/D = 0$, g_z (=$g_\parallel$) = 2.02, g_y = g_x (=$g_\perp$) = 2.24, $A_\parallel$ = 9 · 10^{-4} cm^{-1}, line width = 4 and 21 mT for parallel and perpendicular, respectively.

rhombic symmetry in a nonpolar solvent in analogy with the cation bonding motif in the X-ray structures. The sodium ion is unable to be solvated separately from the complex anion in benzene solution, whereas it is possible in CH_3CN solution thus giving an idealized axial symmetry of the complex anion.

CONCLUSIONS

In summary, two novel tripodal ligands, $(BIMPN^{Mes,Ad,Me})^-$ and $(MIMPN^{Mes,Ad,Me})^{2-}$, combining NHC carbene and phenolate oxygen donors, were synthesized in this study. These chelators complete the N-anchored ligands series with donor functionalities ranging from tris(carbene) to tris(phenolate). The coordination chemistry of these mixed donor ligand systems and that of the all-phenolate system $(^{Ad,Me}ArO_3)N^{3-}$ are reported for divalent Mn, Fe, and Co ions. The ligands and complexes presented here were characterized by single-crystal X-ray diffraction studies, IR, UV/vis spectroscopy, and ^{1}H NMR spectroscopy.

Variable-temperature SQUID magnetization measurements in the range from 2 to 300 K confirm *high-spin* ground states for all complexes, and that the zero-field-splitting parameter $|D|$ increases going from the Mn, to Fe, to Co complexes. ^{57}Fe Mössbauer spectroscopy of Fe(II) complexes **3**, **4**, **8**, and **11** revealed a clear trend toward higher isomer shift δ as carbenes are substituted in the ligand series from tris(carbene) toward tris(phenolate).

The complexes' crystal structures reveal the different steric demand of the ligands. Particularly, the molecular structure of **1**—in which a pyridine molecule is situated next to the Mn−Cl bond—and those of azide complexes **2**, **4**, and **6** demonstrate the mixed ligand's flexibility, and, in contrast to the

corresponding TIMEN^R ligands, their potential to allow side access to the reactive center for organic substrates.

The complete ligand series offers excellent tunability of the electronic and steric environment at the metal center of the complexes, allowing adjustment of the complexes' reactivity. Additionally, the modular synthesis of the mixed ligands allows a combination of different substituents on the NHC and phenolate moieties. We are currently exploring the complexes' capacity for small molecule activation. Studies of the electrochemical and chemical redox behavior are underway. This work includes photolysis experiments of azide complexes **2**, **4**, and **6** for the synthesis of potentially catalytically active nitride complexes.

ASSOCIATED CONTENT

ⓈSupporting Information

Synthetic and analytical details, magnetization data and simulation parameters, and crystallographic details. This material is available free of charge via the Internet at http://pubs.acs.org.

AUTHOR INFORMATION

Corresponding Author
*E-mail: karsten.meyer@fau.de. Fax: (+49) 9131-852-7367.

Notes
The authors declare no competing financial interest.

REFERENCES

(1) Schrock, R. R. *Acc. Chem. Res.* **1997**, *30*, 9−16.
(2) Yandulov, D. V.; Schrock, R. R. *Science* **2003**, *301*, 76−78.
(3) Schrock, R. R. Catalytic Reduction of Dinitrogen to Ammonia by Molybdenum. In *Catalysis without Precious Metals*; Bullock, R. M., Ed.; Wiley-VCH Verlag GmbH & Co. KGaA: Weinheim, Germany, 2010; pp 25−50.
(4) Shook, R. L.; Peterson, S. M.; Greaves, J.; Moore, C.; Rheingold, A. L.; Borovik, A. S. *J. Am. Chem. Soc.* **2011**, *133*, 5810−5817.
(5) Smith, J. M.; Subedi, D. *Dalton Trans.* **2012**, *41*, 1423−1429.
(6) Tolman, W. B. *Activation of Small Molecules: Organometallic and Bioinorganic Perspectives*; Wiley-VCH: Weinheim, Germany, 2006.
(7) Saouma, C. T.; Peters, J. C. *Coord. Chem. Rev.* **2011**, *255*, 920−937.
(8) Betley, T. A.; Wu, Q.; Voorhis, T. V.; Nocera, D. G. *Inorg. Chem.* **2008**, *47*, 1849−1861.
(9) Brown, S. D.; Betley, T. A.; Peters, J. C. *J. Am. Chem. Soc.* **2004**, *125*, 322−323.
(10) Moret, M. E.; Peters, J. C. *Angew. Chem., Int. Ed.* **2011**, *50*, 2063−2067.
(11) Jenkins, D. M.; Betley, T. A.; Peters, J. C. *J. Am. Chem. Soc.* **2002**, *124*, 11238−11239.
(12) Betley, T. A.; Peters, J. C. *J. Am. Chem. Soc.* **2004**, *126*, 6252−6254.
(13) Licini, G.; Mba, M.; Zonta, C. *Dalton Trans.* **2009**, 5265−5277 and references therein.
(14) Hu, X.; Meyer, K. *J. Organomet. Chem.* **2005**, *690*, 5474−5484.
(15) Whiteoak, C. J.; Martin, E.; Belmonte, M. M.; Benet-Buchholz, J.; Kleij, A. W. *Adv. Synth. Catal.* **2012**, *354*, 469−476.

(16) Lam, O. P.; Anthon, C.; Meyer, K. *Dalton Trans.* **2009**, 9677–9691 and references therein.

(17) Vogel, C.; Heinemann, F. W.; Sutter, J.; Anthon, C.; Meyer, K. *Angew. Chem., Int. Ed.* **2008**, *47*, 2681–2684.

(18) Kropp, H.; King, A. E.; Khusniyarov, M. M.; Heinemann, F. W.; Lancaster, K. M.; DeBeer, S.; Bill, E.; Meyer, K. *J. Am. Chem. Soc.* **2012**, *134*, 15538–15545.

(19) Hu, X.; Castro-Rodriguez, I.; Meyer, K. *J. Am. Chem. Soc.* **2004**, *126*, 13464–13473.

(20) Hu, X.; Meyer, K. *J. Am. Chem. Soc.* **2004**, *126*, 16322–16323.

(21) Vogel, C. S. *High- and Low-Valent tris-N-Heterocyclic Carbene Iron Complexes: A Study of Molecular and Electronic Structure*; Springer: Heidelberg, 2012.

(22) Vogel, C. S.; Heinemann, F. W.; Khusniyarov, M. M.; Meyer, K. *Inorg. Chim. Acta* **2010**, *364*, 226–237.

(23) Such as bidentate NHC/phenolates, (see, for example, refs 23a and 23b), vaulted, 4-coordinate bis(NHC-phenolates) (ref 23c), or pincer-type ligands with an OCO binding motif (O = phenolate, C = NHC) (refs 23d–23g): (a) Liddle, S. T.; Edworthy, I. S.; Arnold, P. L. *Chem. Soc. Rev.* **2007**, *36*, 1732. (b) Kong, Y.; Xu, S.; Song, H.; Wang, B. *Organometallics* **2012**, *31*, 5527–5532. (c) Komiya, N.; Yoshida, A.; Naota, T. *Inorg. Chem. Commun.* **2013**, *27*, 122–126. (d) Aihara, H.; Matsuo, T.; Kawaguchi, H. *Chem. Commun.* **2003**, 2204. (e) Zhang, D.; Aihara, H.; Watanabe, T.; Matsuo, T.; Kawaguchi, H. *J. Organomet. Chem.* **2007**, *692*, 234–242. (f) Bellemin-Laponnaz, S.; Welter, R.; Brelot, L.; Dagorne, S. *J. Organomet. Chem.* **2009**, *694*, 604–606. (g) Arnold, P. L.; Wilson, C. *Inorg. Chim. Acta* **2007**, *360*, 190–196.

(24) Despagnet-Ayoub, E.; Miqueu, K.; Sotiropoulos, J.-M.; Henling, L. M.; Day, M. W.; Labinger, J. A.; Bercaw, J. E. *Chem. Sci.* **2013**, *4*, 2117–2121.

(25) Gademann, K.; Chavez, D. E.; Jacobsen, E. N. *Angew. Chem., Int. Ed.* **2002**, *41*, 3059–3061.

(26) Flassbeck, C.; Wieghardt, K. *Z. Anorg. Allg. Chem.* **1992**, *608*, 60–68.

(27) For the coordinated azide ligand, a total of three absorption bands are expected in the IR vibrational spectrum, originating from the symmetric $\nu_s(N_3)$ and the asymmetric $\nu_{as}(N_3)$ stretching vibrations at around 1300 and 2000 cm^{-1}, respectively. The third absorption is assigned to the deformation vibration $\nu(N_3)$ at approximately 400 cm^{-1}. Thus, strictly speaking, for a mono-azide metal complex, only *one* $\nu_{as}(N_3)$ absorption band is expected in the 2000 cm^{-1} region. We note, however, that the azide complexes of the bis(carbene) mono(phenolate) ligand in complexes **2**, **4**, and **6** crystallize with two independent molecules per unit cell and that the chelate allows for a variety of M–N$_3$ conformations. This likely results in a number of different $\nu_{as}(N_3)$ vibration frequencies and absorption bands. In addition, because of interactions with the "matrix", such as KBr in the solid state or a solvent molecule in solution, the number of absorption bands can vary. In a simple, classic case of a coordinated azide, e.g., TlN$_3$, Dehnicke reports (Dehnicke, K. *Z. Anorg. Allg. Chem.* **1974**, *409*, 311) two absorption bands centered at 2037 and 2000 cm^{-1} for $\nu_{as}(N_3)$ and two bands at 1328 and 1319 cm^{-1} for the $\nu_s(N_3)$ vibration. We note that the solution IR spectrum of **6** also shows two vibrational bands at 2081 and 2041 cm^{-1} (see the Supporting Information, Figure S34).

(28) For comparison of Mn–C$_{carb}$ bond lengths, see, for example: (a) Hock, J. H.; Schaper, L.-A.; Herrmann, W. A.; Kühn, F. E. *Chem. Soc. Rev.* **2013**, *42*, 5073–5089. (b) Abernethy, C. D.; Cowley, A. H.; Jones, R. A.; Macdonald, C. L. B.; Shukla, P.; Thompson, L. K. *Organometallics* **2001**, *20*, 3629–3631. (c) Chai, J.; Zhu, H.; Most, K.; Roesky, H. W.; Vidovic, D.; Schmidt, H.-G.; Noltemeyer, M. *Eur. J. Inorg. Chem.* **2003**, 4332–4337. (d) Chai, J.; Zhu, H.; Peng, Y.; Roesky, H. W.; Singh, S.; Schmidt, H.-G.; Noltemeyer, M. *Eur. J. Inorg. Chem.* **2004**, 2673–2677. (e) Pugh, D.; Wright, J. A.; Freeman, S.; Danopoulos, A. A. *Dalton Trans.* **2006**, 775–782. (f) Kennedy, A. R.; Klett, J.; Mulvey, R. E.; Robertson, S. D. *Eur. J. Inorg. Chem.* **2011**, 4675–46790. (g) Musgrave, R. A.; Turbervill, R. S. P.; Irwin, M.; Goicoechea, J. M. *Angew. Chem., Int. Ed.* **2012**, *51*, 10832–10835. (h) Kropp, H.; King, A. E.; Khusniyarov, M. M.; Heinemann, F. W.;

Lancaster, K. M.; DeBeer, S.; Bill, E.; Meyer, K. *J. Am. Chem. Soc.* **2012**, *134*, 15538–15544.

(29) For comparison of Fe–C$_{carb}$ bond lengths, see, for example: (a) Louie, J.; Grubbs, R. *J. Chem. Commun.* **2000**, 1479–1480. (b) Danopoulos, A. A.; Tsoureas, N.; Wright, J. A.; Light, M. E. *Organometallics* **2004**, *23*, 166–168. (c) Vogel, C.; Heinemann, F. W.; Sutter, J.; Anthon, C.; Meyer, K. *Angew. Chem., Int. Ed.* **2008**, *47*, 2681–2684. (d) Scepaniak, J. J.; Fulton, M. D.; Bontchev, R. P.; Duesler, E. N.; Kirk, M. L.; Smith, J. M *J. Am. Chem. Soc.* **2008**, *130*, 10515–10517. (e) Danopoulos, A. A.; Pugh, D.; Smith, H.; Saßmannshausen, J. *Chem.—Eur. J.* **2009**, *15*, 5491–5502. (f) Scepaniak, J. J.; Margarit, C. G.; Harvey, J. N.; Smith, J. M. *Inorg. Chem.* **2011**, *50*, 9508–9517. (g) Scepaniak, J. J.; Harris, T. D.; Vogel, C. S.; Sutter, J.; Meyer, K.; Smith, J. M. *J. Am. Chem. Soc.* **2011**, *133*, 3824–3827. (h) Xiang, L.; Xiao, J.; Deng, K. *Organometallics* **2011**, *30*, 2018–2025. (i) Zlatogorsky, S.; Muryn, C. A.; Tuna, F.; Evans, D. J.; Ingleson, M. J. *Organometallics* **2011**, *30*, 4974–4982. (j) Meyer, S.; Orben, C. M.; Demeshko, S.; Dechert, S.; Meyer, F. *Organometallics* **2011**, *30*, 6692–6702. (k) Day, B. M.; Pugh, T.; Hendriks, D.; Guerra, C. F.; Evans, D. J.; Bickelhaupt, F. M.; Layfield, R. A. *J. Am. Chem. Soc.* **2013**, *135*, 13338–13341.

(30) The molecular structures of **5-Cl** and **5-PF$_6$** are very similar; therefore, only one structure is discussed here and the other is given in the Supporting Information.

(31) Details for the synthesis, crystallography, and spectroscopy of this complex will be reported elsewhere.

(32) Because of the additional axial ligands, the other (BIMPN^{Mes,Ad,Me})$^-$ complexes' molecular structures are not directly comparable.

(33) Kaim, W. *Eur. J. Inorg. Chem.* **2012**, 343–348.

(34) Shimazaki, Y.; Yamauchi, O. *Indian J. Chem.* **2010**, *50A*, 383–394.

(35) Ray, K.; Petrenko, T.; Wieghardt, K.; Neese, F. *Dalton Trans.* **2007**, 1552–1566.

(36) For comparison of bond lengths in coordinated phenolates and phenoxyl racials, see, for example: (a) Bill, E.; Bothe, E.; Chaudhuri, P.; Chlopek, K.; Herebian, D.; Kokatam, S.; Ray, K.; Weyhermuller, T.; Neese, F.; Wieghardt, K. *Chemistry* **2004**, *11*, 204–224. (b) Sokolowski, A.; Bothe, E.; Bill, E.; Weyhermüller, T.; Wieghardt, K. *Chem. Commun.* **1996**, 1671–1672.

(37) Gütlich, P.; Bill, E.; Trautwein, A. X. *Mössbauer Spectroscopy and Transition Metal Chemistry*; Springer: Heidelberg, 2011.

(38) Greenwood, N. N.; Gibb, T. C. *Mössbauer Spectroscopy*; Chapman and Hall: London, 1971.

(39) The synthesis and characterization by Dr. Carola Vogel; see the Supporting Information.

(40) Hu, X.; Castro-Rodriguez, I.; Olsen, K.; Meyer, K. *Organometallics* **2004**, *23*, 755–764.

(41) See the Supporting Information for the synthesis and characterization of the (^{tBu,tBu}ArO)$_3$N^{3-} complex of Co and its two crystal structures.

(42) Only simulations with nonzero *E* result in reasonable *g*-values. To determine parameters more accurately, it would be necessary to perform an experiment at another frequency such as Q-band.